

Chapter 7

The Brownian Dynamics Method Applied

Contents

7.1	Diffusion in a Linear Potential	103
7.2	Diffusion in a Harmonic Potential	104
7.3	Harmonic Potential with a Reactive Center	107
7.4	Free Diffusion in a Finite Domain	107
7.5	Hysteresis in a Harmonic Potential	108
7.6	Hysteresis in a Bistable Potential	112

In this chapter we apply the Brownian dynamics method to motion in prototypical force fields. We consider first the cases of constant and linear force fields for which analytical solutions exist which allow one to test the accuracy of the Brownian dynamics method. We consider, in particular, statistical uncertainties inherent in Brownian dynamic simulations. Estimates for the statistical error of observables are derived. We consider also examples with reflecting and absorbing boundaries. Finally we describe hysteresis in a harmonic and in a bistable potential. The later case is not amenable to analytical solutions and, thus, the approach described constitutes a truly useful application of the Brownian dynamics method.

7.1 Diffusion in a Linear Potential

As a first example we consider the simple scenario of diffusion in a linear potential $V(x) = ax$ with boundaries at infinity. In this model the diffusive particles are subject to a constant force $F(x) = -a$. One obtains with (4.17) the Fokker Planck respectively Smoluchowski diffusion equation

$$\partial_t p(x, t|x_0, t_0) = D (\partial_x^2 + \beta a \partial_x) p(x, t|x_0, t_0) . \quad (7.1)$$

By comparing (7.1) with (6.1) one identifies the drift coefficient $A(x, t) = -D\beta a$ and the noise coupling coefficient $B(x, t) = \sqrt{2D}$. Both coefficients are constant and again as in the free diffusion model assumptions (6.6) and (6.7) are met for any step size $\Delta t = t_{i+1} - t_i$.

The random numbers needed in the Brownian dynamics procedure (6.20) are generated according to (6.18) with the mapping

$$\tilde{r}_k(x, t) = \sqrt{2D\Delta t} r_k - D\beta a \Delta t + x \quad (7.2)$$

The random number probability density distribution is

$$p(\tilde{r}(x, t)) = \frac{1}{\sqrt{4\pi D \Delta t}} \exp\left(-\frac{(\tilde{r}(x, t) + D\beta a \Delta t - x)^2}{4 D \Delta t}\right). \quad (7.3)$$

The end points $x(t)$ of a sample path in (6.20) result from chains of random numbers given in (7.2). This chain of random numbers $\tilde{r}_k(x_k, t_k)$ can be rewritten as a sum

$$\begin{aligned} x(t = t_N) &= \tilde{r}_N(\dots \tilde{r}_1(\tilde{r}_0(x_0, t_0), t_1) \dots, t_N) \\ &= -D\beta a (t - t_0) + \sqrt{2D\Delta t} \sum_{k=1}^N r_k. \end{aligned} \quad (7.4)$$

The only difference between equation (7.4) and equation (6.29) of the free diffusion model is the term $-D\beta a t$. One apparently generates the same sample trajectories as in the case of free diffusion except for a displacement. The endpoints $x(t)$ of a trajectory are shifted by $-D\beta a t$.

Due to this similarity we are not going to repeat a bin count as done in section 6.4. Instead we investigate a new observable. We consider a measurement Q_{x_m} that renders the probability of finding a particle beyond a certain point x_m on the x -axes. The sensitivity function of such an observable is $q_{x_m}(x) = \Theta(x - x_m)$. We will now estimate the number M of sample trajectories needed to determine

$$q_{x_m}(t|x_0, t_0) = \int_{\Omega} dx \Theta(x - x_m) p(x, t|x_0, t_0). \quad (7.5)$$

The value range of observable Q_{x_m} is the interval $[0, 1]$. Hence, the variance $\langle\langle q_{x_m}^2(t|x_0, t_0) \rangle\rangle$ can not exceed 1. One can therefore assume, according to (6.37), that the standard deviation of $\bar{q}_{x_m}(t|x_0, t_0)$ is less than $1/\sqrt{M}$. To push the statistical error of $\bar{q}_{x_m}(t|x_0, t_0)$ below a margin of $\pm 2\%$ one has to simulate and sample ($M = 2500$) trajectories. The result of such a simulation is displayed in Figure 7.1. The plot describes the time dependent increase in probability for finding a particle beyond x_m . The units are chosen so that $D = 1$. The force constant a is set equal $-2/\beta$ and x_m is located at $+1$.

7.2 Diffusion in a Harmonic Potential

We alter the previous Brownian dynamics simulation by implementing a harmonic potential $V(x) = \frac{k}{2} x^2$. This harmonic potential introduces a decisive difference to the previously used examples. It requires the introduction of intermediate times t_i in the simulation of stochastic trajectories (6.20) since in this case $A(x, t)$ is not constant. The more intermediate times t_i and the smaller the time steps Δt the better the simulation. We will examine the impact of the time step length Δt on the numerical results and derive guidelines for the right choice of Δt .

Inserting the harmonic force $F(x) = -kx$ into the Smoluchowski diffusion equation (4.17) one derives

$$\partial_t p(x, t|x_0, t_0) = D (\partial_x^2 + \beta k \partial_x x) p(x, t|x_0, t_0). \quad (7.6)$$

Again comparing (7.1) with (6.1) one identifies the drift coefficient $A(x, t) = -D\beta kx$ and the noise coupling coefficient $B(x, t) = \sqrt{2D}$. Note that $A(x, t)$ is no longer a spatial constant. One, thus, has to pay special attention to assumptions (6.6) and (6.7).

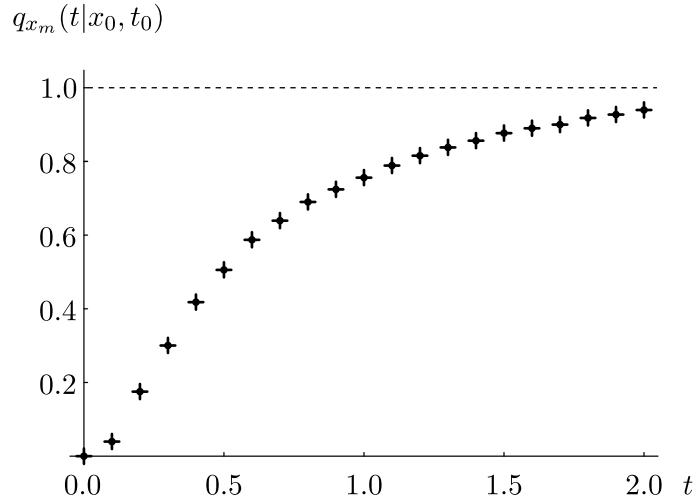


Figure 7.1: The plot displays the readings of observable Q_{x_m} according to (7.5) in a Brownian dynamics calculation (7.4) with 2500 trajectories.

Each trajectory step in a Brownian Dynamics simulation is exact for a linear potential $V(x) = ax$. During a time step Δt a simulated particle diffuses as if the potential $V(x)$ extrapolates linearly. One has to assure that this linear extrapolation is a good approximation for the average spatial simulation step Δx given in (6.5). The difference $\Delta V(x)$ between the exact and the linearly extrapolated potential is given by

$$\Delta V(x + \Delta x) = V(x + \Delta x) - [V(x) + V'(x) \Delta x] . \quad (7.7)$$

Conversely one can determine the approximation radius $\pm \Delta x$ for a given potential deviation $\Delta V(x + \Delta x)$.

$$\Delta x = \frac{V(x + \Delta x) - V(x) - \Delta V(x + \Delta x)}{V'(x)} . \quad (7.8)$$

Hence, if we intend to keep the approximation of $V(x)$ within the interval $[V(x) - \Delta V(x), V(x) + \Delta V(x)]$ we can derive the necessary upper limit for the spatial step size Δx according to (7.8) and determine the corresponding upper limit for the temporal step size

$$\Delta t = \frac{B(x, t) + 2|A(x, t)| \Delta x - \sqrt{B^2(x, t) + 4|A(x, t)| B(x, t) \Delta x}}{2A^2(x, t)} . \quad (7.9)$$

We consider a specific example. We set D and β equal 1, thus measuring the potential in units of the average thermal energy $1/\beta$ and relating the units of space and time via D . Within these units we simulate trajectories with the initial position $x_0 = 1$ in a potential with $k = 6$. If one intends to keep the approximation of $V(x)$ within 10% of the thermal energy $1/\beta$, one can determine the upper limit for the spatial step size with (7.8) and derive $\Delta x \approx 0.2$.

To obtain the corresponding upper limit for the temporal step size Δt with (7.9), one has to estimate maximum values for $|A(x, t)|$ and $B(x, t)$. Assuming an effective diffusion domain of $[-2, 2]$ one finds $|A(x, t)| \leq 2kD\beta$ and $B(x, t) = \sqrt{2D}$ and consequently $\Delta t \approx 0.01$. Simulation results with these parameters are shown in Figures 7.2. The three bar charts display the time evolution of a bin count at times $t = 0.02, 0.08,$ and 0.40 . The bin count, based on 1000 trajectories, exhibits 20 bins with a width of 0.2 each. The bin count approximates probability distribution $p(x, t|1, 0)$ with the analytical solution (3.142), which is superimposed for comparison.

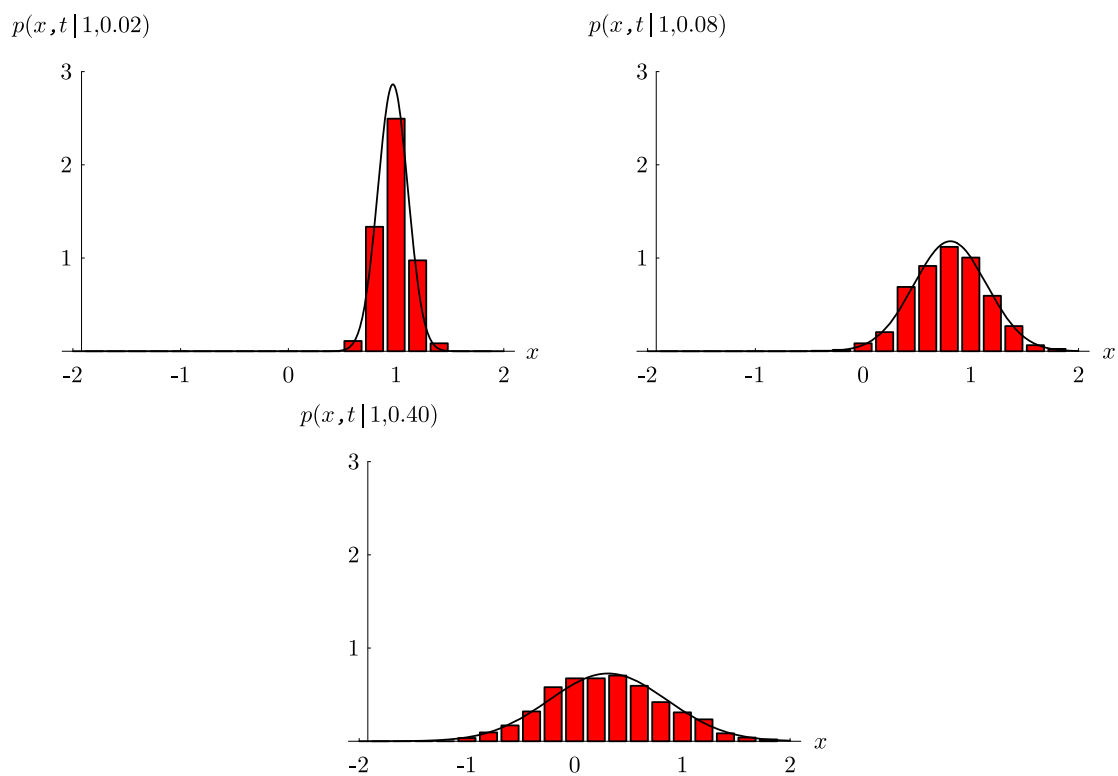


Figure 7.2: The bar charts depict bin counts of a Brownian Dynamics simulation with the harmonic potential $V(x) = \frac{k}{2}x^2$. The three figures display the probability distribution $p(x, t | 1, 0)$ of the simulated trajectories at times $t = 0.02, 0.08$, and 0.40 . The analytical results (3.142) are superimposed for comparison.

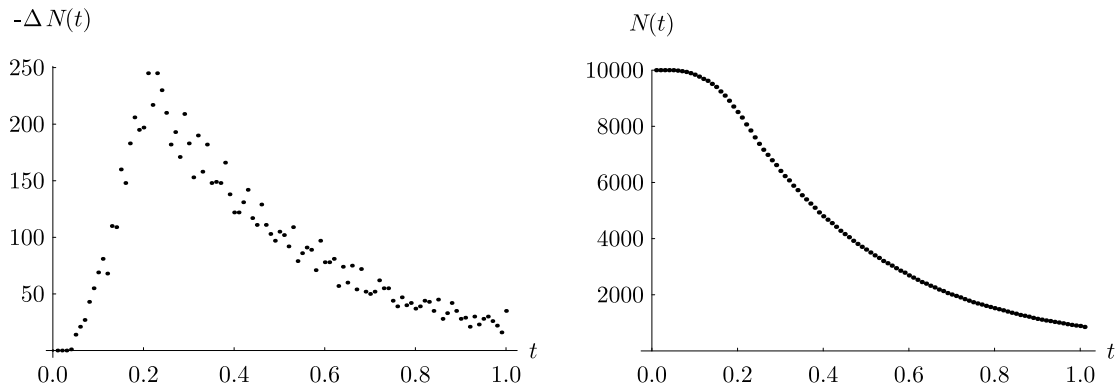


Figure 7.3: The number of particles absorbed by boundary $x = 0$ per time step Δt (left). The number $N(t)$ of particles remaining in the system (right).

7.3 Harmonic Potential with a Reactive Center

We refine the harmonic potential example by introducing a reactive center at $x = 0$. We thereby address the issue of reactive boundary conditions in Brownian dynamics.

In a one-dimensional model a reactive site within a potential is equivalent to a reactive boundary. The particles cannot cross the reactive site without being absorbed or reflected. Thus, for particles, never being able to reach the other side, a reactive site appears as wall or boundary.

There is a simple and intuitive way to incorporate reactive boundaries in a Brownian dynamic calculation. At each time step Δt one determines the number of trajectories crossing the reactive wall. One then removes a certain percentage of trajectories from the ensemble depending on reaction rate of the boundary. The remaining percentage is reflected according to the rules developed in section 6.5.

To verify the drain of particles one can calculate the particle number $N(t)$ and determine the time-dependence by counting the remaining particles at different times t .

We quickly consider a particular example. Assume a sink at the center of the harmonic potential. This sink is in effect a completely absorbing wall. Thus, in a simulation we simply remove all particles crossing this boundary. With the same parameters as in the calculation of the previous section we compute the particle flux $-\Delta N(t)/\Delta t$ absorbed by the sink at $x = 0$ and we determine the number $N(t)$ of particles still present in the system. The results of a simulation with $N(0) = 10000$ initial particles are plotted with respect to time t in Figure 7.3.

7.4 Free Diffusion in a Finite Domain

We revisit the model of free diffusion in a finite domain $\Omega = [0, a]$ with reflective boundaries. We solved this model analytically in section 3.5.

Under the condition $D dt \ll a^2$ one can use the solutions (6.56) for the conditional probability distribution $p(x, t_0 + dt | x_0, t_0)$ at the left and right boundary. These solutions in the half-spaces $[0, \infty[$ and $] -\infty, a]$ can be patched together at $x = a/2$.

$$p(x, t_0 + dt | x_0, t_0) \approx \frac{1}{\sqrt{4\pi D dt}} \begin{cases} \exp\left[-\frac{(x-x_0)^2}{4D dt}\right] + \exp\left[-\frac{(x+x_0)^2}{4D dt}\right] & x \leq \frac{a}{2} \\ \exp\left[-\frac{(x-x_0-a)^2}{4D dt}\right] + \exp\left[-\frac{(x+x_0-a)^2}{4D dt}\right] & x > \frac{a}{2} \end{cases}. \quad (7.10)$$

A distribution of this form results from a Wiener process which is modified, in that the paths with $x < 0$ and $x > a$ are ‘reflected’ back into the domain $\Omega = [0, a]$. Hence, the Wiener process in the interval $[0, a]$ is defined as in (6.57) and one can write

$$x(t + \Delta t) = \begin{cases} x(t) + \sqrt{2D\Delta t} r(t) & , \text{ if } x(t) + \sqrt{2D\Delta t} r(t) \in \Omega \\ -x(t) - \sqrt{2D\Delta t} r(t) & , \text{ if } x(t) + \sqrt{2D\Delta t} r(t) < 0 \\ 2a - x(t) - \sqrt{2D\Delta t} r(t) & , \text{ if } x(t) + \sqrt{2D\Delta t} r(t) > a \end{cases} . \quad (7.11)$$

The function $p(x, t|x_0, t_0)$ is the probability density of the stochastic trajectories $x(t)$, subject to the initial condition $x(t_0) = x_0$. By simulating on a computer a fairly large number of random walks according to (7.11), one can determine, within the limits of statistical and numerical errors, the probability distribution $p(x, t|x_0, t_0)$. For this purpose one performs a bin count as in section 6.4.

To perform a simulation of an ensemble of stochastic trajectories $x(t)$ we choose specific parameters. We set the unit of length to be a and the unit of time to be D/a^2 ; hence $a = 1$ and $D = 1$. We choose an arbitrary value for x_0 and determine a Δt satisfying $D\Delta t \ll a^2$.

According to the scheme described above, one starts the actual Brownian Dynamics simulation of ($N = 1000$) trajectories at $x_0 = a/4$. To approximate $p(x, t|x_0, t_0)$ one can perform a bin count after $(t - t_0)/\Delta t$ number of time steps Δt by counting and recording the numbers of trajectories in each bin. One can then estimate $p(x, t|x_0, t_0)$ in each bin with equation (6.40). Results of an actual simulation at $t = 0.01, 0.03, 0.1, 0.3$ are presented in Figures 7.4. The bin counts exhibit 20 bins with a base length of $0.05a$ each. The analytical solution (3.142) for $p(x, t|x_0, 0)$ are superimposed for comparison.

7.5 Hysteresis in a Harmonic Potential

For an application of the Brownian Dynamics method we consider now particles moving in a one-dimensional potential $V(x)$ subject to a driving force $F_d(t)$ with a sinusoidal time-dependence $\sin(\omega t)$. This example allows us to investigate the properties of hysteresis, which arises, for example, when proteins are subjected to time-dependent electric fields.

Before providing numerical answers we have to identify the right questions and the important aspects of hysteresis. Since we consider systems governed by the Smoluchowski equation (4.17) which arises from a Langevin equation with frictional forces the external forces lead to the dissipation of energy leading to a net energy consumption of the system in the case of periodic forces. The energy dE delivered through an external force field to a single particle during an infinitesimal time step dt is given by the scalar product of the particles path segment dx and the exerted force F_d . The average energy $\langle dE \rangle$ delivered to the particle ensemble is therefore

$$\begin{aligned} \langle dE \rangle &= \langle F_d \cdot dx \rangle \\ &= F_d \cdot \langle dx \rangle . \end{aligned} \quad (7.12)$$

The system compensates the energy uptake with an energy loss via the stochastic interactions. The aim of our numerical calculations will be to quantify and to investigate this energy consumption. We will base the subsequent calculations on the following premises. For times t much larger than the relaxation times of the system the particle ensemble will assume a so-called *asymptotic state* in which it will exhibit the same temporal cyclic variation as the driving force $F_d(t)$. In such an

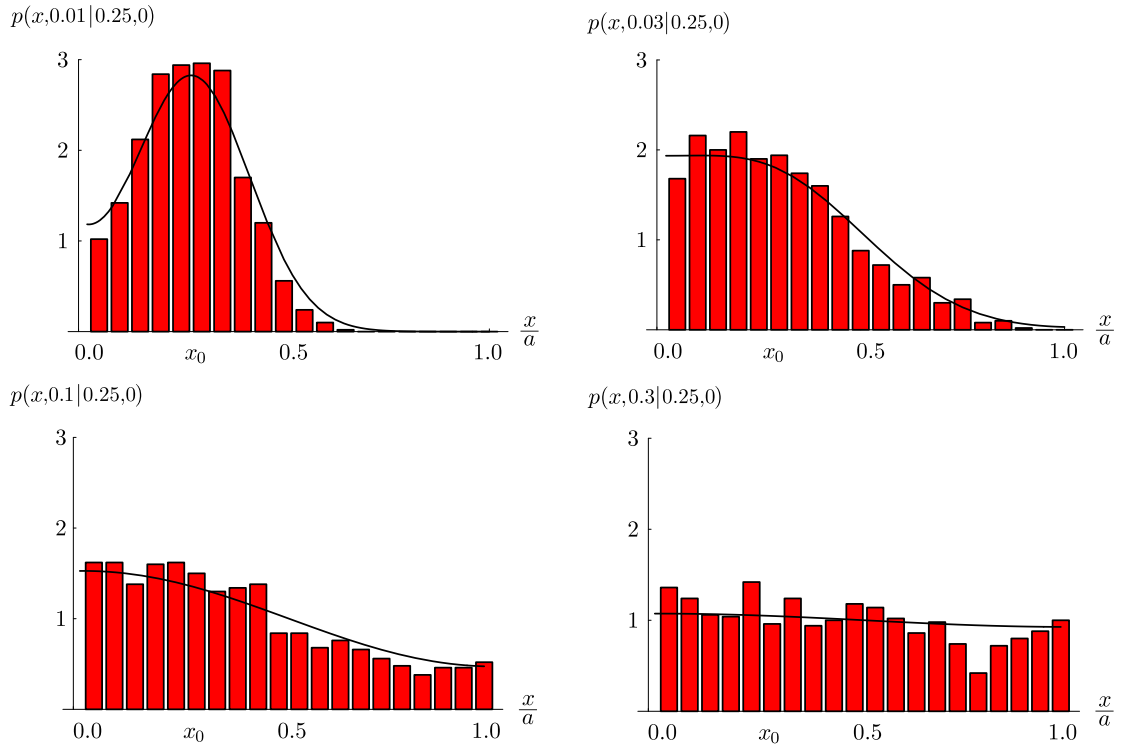


Figure 7.4: These bin counts present a Brownian dynamics simulation with 1000 particles diffusing according to (7.11) in an interval $[0, a]$ with reflective boundaries.

asymptotic state the energy gain and loss will compensate each other over each cycle and one can, thus, measure the energy dissipation by observing the energy uptake dE .

For a periodic asymptotic state it is sufficient to consider the time evolution during just one variation cycle. We therefore focus on the energy uptake E_c during a single cycle. We parameterize the cycle by $\phi = \omega t$ ranging from 0 to 2π and obtain with (7.12) for the energy E_c provided by linear force field $F_d(t) = a \sin(\omega t)$

$$\langle E_c \rangle = a \oint d\sin(\phi) \langle x(\phi) \rangle . \quad (7.13)$$

It is customary to express equation (7.13) in terms of hysteresis \mathcal{H} which is defined as

$$\mathcal{H} = - \oint d\sin(\phi) x(\phi) . \quad (7.14)$$

To proceed we have to choose a particular potential $V(x)$. In this section we first consider the simplest form of a potential, the harmonic potential in conjunction with a linear force field

$$V(x) = \frac{k}{2}x^2 + F_d(t)x , \quad (7.15)$$

$$F_d(t) = a \sin(\omega t) . \quad (7.16)$$

The Fokker-Planck equation determining the time evolution of the probability distribution $p(x, t|x_0, t_0)$ can then be written as

$$\partial_t p(x, t|x_0, t_0) = D (\partial_x^2 + \beta(a \sin(\omega t) + k \partial_x x)) p(x, t|x_0, t_0) . \quad (7.17)$$

To determine the hysteresis \mathcal{H} as in (7.17) it is beneficial to substitute t by ϕ . We derive

$$\partial_\phi p(x, \phi | x_0, \phi_0) = \frac{D}{\omega} (\partial_x^2 + \beta (a \sin(\phi) + k \partial_x x)) p(x, \phi | x_0, \phi_0). \quad (7.18)$$

Before solving equation (7.18) numerically we will quickly outline the analytical solution. For the solution of the Smoluchowski equation for the harmonic potential without a driving force one assumes the functional form

$$p(x, \phi) = \sqrt{\frac{\beta k}{2\pi}} \exp\left[-\frac{1}{2} \beta k (x - \langle x(\phi) \rangle)^2\right]. \quad (7.19)$$

Substituting (7.19) into (7.18) one obtains an ordinary differential equation for the mean path $\langle x(\phi) \rangle$.

$$\partial_\phi \langle x(\phi) \rangle = -\beta \frac{D}{\omega} (k \langle x(\phi) \rangle + a \sin \phi). \quad (7.20)$$

The solution of (7.20) is

$$\langle x(\phi) \rangle = -\frac{a \beta D / \omega}{k^2 (\beta D / \omega)^2 + 1} e^{-k (\beta D / \omega) \phi} + a \frac{(\beta D / \omega) \cos \phi - k (\beta D / \omega)^2 \sin \phi}{k^2 (\beta D / \omega)^2 + 1}. \quad (7.21)$$

In determining the hysteresis we consider only the asymptotic state with $\omega t = \phi \rightarrow \infty$. In this limit the first term of (7.21) vanishes and one obtains

$$\langle x(\phi) \rangle = a \frac{(\beta D / \omega) \cos \phi - k (\beta D / \omega)^2 \sin \phi}{k^2 (\beta D / \omega)^2 + 1}. \quad (7.22)$$

This expression is all one needs to evaluate (7.14) and to determine the mean hysteresis

$$\begin{aligned} \langle \mathcal{H} \rangle &= - \oint d \sin \phi \langle x(\phi) \rangle \\ &= \oint d \sin \phi a \frac{(\beta D / \omega) \cos \phi - k (\beta D / \omega)^2 \sin \phi}{k^2 (\beta D / \omega)^2 + 1} \\ &= \frac{\pi a \beta D / \omega}{k^2 (\beta D / \omega)^2 + 1}. \end{aligned} \quad (7.23)$$

Having derived an analytical description we turn now to the application of the Brownian Dynamics method which should reproduce the result (7.23). We determine first the mean path $\langle x(\phi) \rangle$ numerically and evaluate then (7.14). For the evaluation of the mean path we proceed in the same way as in the previous sections. Comparing (7.18) and (6.1) we identify the drift coefficient $A(x, \phi) = -D \beta (k x + a \sin(\phi)) / \omega$ and the noise coupling coefficient $B(x, \phi) = \sqrt{2D/\omega}$. The resulting equation for the numerical integration of a particle trajectory is

$$x(\phi + \Delta\phi) = x(\phi) - \frac{D \beta}{\omega} (a \sin(\phi) + k x) \Delta\phi + \sqrt{\frac{2D}{\omega}} \Delta\phi. \quad (7.24)$$

We start the Brownian Dynamics simulation with reasonably small phase steps $\Delta\phi$ and hope that assumptions (6.6) and (6.7) are met. We, thus, obtain rough results which we will refine later. The results of a simulation with 10000 particles initially distributed according to the thermal equilibrium distribution of the harmonic potential (see (4.86) or (7.19))

$$p_0(x, \phi = 0) = \sqrt{\frac{k \beta}{2\pi}} \exp\left(-\frac{k \beta x^2}{2}\right) \quad (7.25)$$

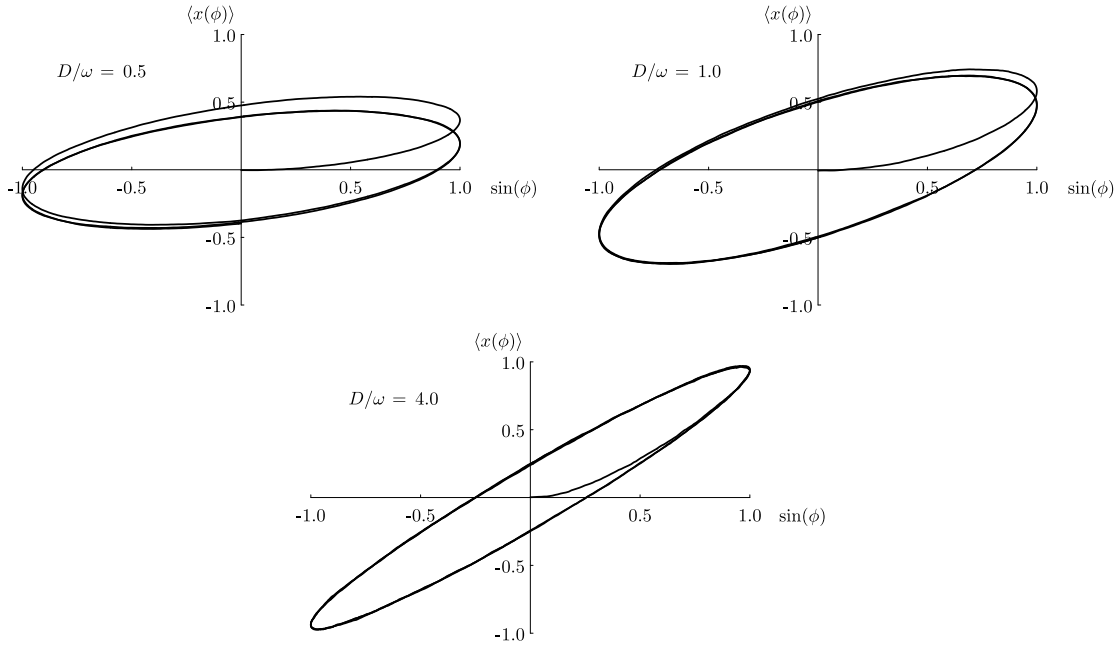


Figure 7.5: Mean trajectories of 10000 Brownian particles simulated according to (7.24) with $\Delta\phi = 0.002\pi$, $a = 6/\beta$, $k = 6/\beta$ and $2\pi D/\omega = 0.5, 1.0, 4.0$ (arbitrary spatial unit).

are presented in Figure 7.5. These graphs display the mean trajectory $\langle x(\phi) \rangle$ with respect to $\sin(\phi)$ varying ϕ from 0 to 6π for different values of D/ω .

The mean trajectory $\langle x(\phi) \rangle$ starts at the origin of the coordinate system of $\langle x \rangle$ and ϕ and converges after the first one or two cycles on an ellipse. The area encircled by the ellipse is the integral (7.14) and, hence represents the hysteresis \mathcal{H} and energy consumption E_c . One can determine the encircled area numerically by applying standard numerical integration methods like the *closed Newton-Cotes Formula* [37] to (7.14).

Before we proceed we have to investigate the influence of the step size $\Delta\phi$ on our numerical results. For this purpose we calculate $\langle \mathcal{H} \rangle$ for different step size values $\Delta\phi$. The results of $\langle \mathcal{H} \rangle$ with $2\pi D/\omega = 1$ for $\Delta\phi = 0.002\pi, 0.004\pi, 0.01\pi, 0.02\pi$, and 0.04π are shown in Figure 7.6. One can observe a linear dependence between $\langle \mathcal{H} \rangle$ and $\Delta\phi$. Hence, we can extrapolate to the limit $\Delta\phi \rightarrow 0$ by performing a linear regression. The value of the linear regression at $\Delta\phi = 0$ can be taken as the *true* value of \mathcal{H} , which in this case lies within one per mille of the analytical result $3/((3/\pi)^2 + 1) = 1.56913$ of (7.23).

One can observe in equation (7.23) and in Figures 7.7 that the mean hysteresis $\langle \mathcal{H} \rangle$ varies with respect to D/ω . To elucidate this D/ω -dependence we determine $\langle \mathcal{H} \rangle$ for a sequence of different D/ω values ranging from 0.1 to 5.0. The resulting plot is displayed in Figure 7.7. The numerical and analytical solutions are identical with respect to the resolution in Figure 7.7. The hysteresis $\langle \mathcal{H} \rangle$ reaches a maximum for

$$\frac{D}{\omega} = \frac{1}{\beta k}. \quad (7.26)$$

For higher $\frac{D}{\omega}$ -values or equivalently for lower frequencies ω the ensemble has sufficient time to follow the external force $F_d(t)$ almost instantly. The time delayed response is shorter and the hysteresis $\langle \mathcal{H} \rangle$ is reduced. For lower $\frac{D}{\omega}$ -values or equivalently for higher frequencies ω the system cannot

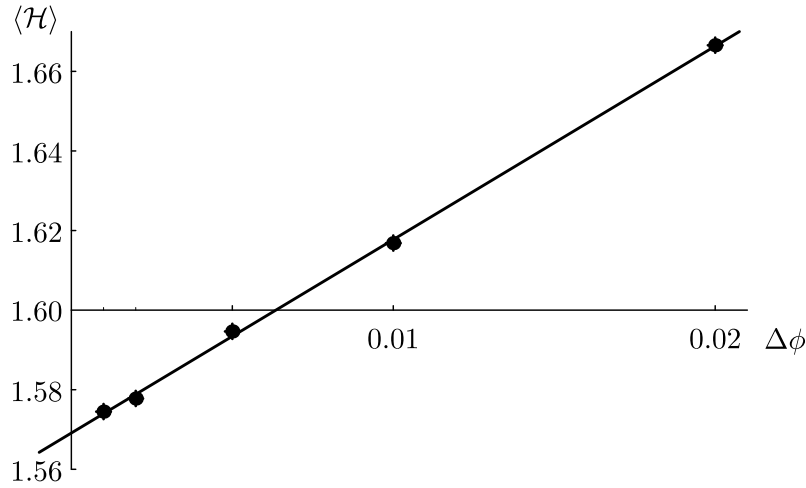


Figure 7.6: $\Delta\phi$ -dependence of the numerical results of the mean hysteresis $\langle \mathcal{H} \rangle$ based on 100000 trajectories. The points mark the results for $\Delta\phi = 0.002\pi, 0.004\pi, 0.01\pi, 0.02\pi$, and 0.04π . The other parameters are $a = 6/\beta$, $k = 6/\beta$ and $2\pi D/\omega = 1$ with respect to some arbitrary spatial unit. The line represents the linear regression of the five numerical results. It allows one to extrapolate the linear dependence between $\langle \mathcal{H} \rangle$ and $\Delta\phi$, and to approximate the hysteresis for the limit $\Delta\phi \rightarrow 0$.

follow the driving force in time. The effect of the driving force thereby cancels itself with each cycle and the amplitude of the mean path $\langle x(\phi) \rangle$ approaches zero. The smaller the amplitude the smaller the hysteresis $\langle \mathcal{H} \rangle$.

7.6 Hysteresis in a Bistable Potential

In our last application of the Brownian Dynamics method we leave the domain of analytically solvable problems and simulate a system accessible only by numerical means. We consider again a system exhibiting hysteresis, but in cases that the observed hysteresis cannot be reconciled with a harmonic potential model. For example, the deflection $x(t)$ of a system does usually not increase linearly with the strength of the external force field $F_d(t)$. A non-linear saturation effect can only be modeled with a potential of fourth or higher order in x . Furthermore one usually observes a remaining deflection in x after switching off the external force $F_d(t)$. The remaining magnetization of an iron core in a transformer is a typical example. Such an effect cannot be modeled with a one-minimum-potential. With no external force the systems would always decay to the thermal equilibrium of its one minimum without sustaining a remaining deflection in time. Hence, to create a model with a remaining deflection one needs to consider a bistable potential.

To investigate the above effects we employ the bistable potential

$$\begin{aligned} V(x) &= \frac{k_1}{4} x^4 - \frac{k_2}{2} x^2 + x F_d(t), \\ F_d(t) &= a \sin(\omega t). \end{aligned} \quad (7.27)$$

For the following simulations we assume the parameters $k_1 = 1/\beta$, $k_2 = 1/\beta$ and $a = 1/2\beta$. We, thus, obtain with (7.27) a potential $V(x)$ that has two minima, one at $x = -1$ and one at $x = 1$ with a barrier of height $1/(4\beta)$ inbetween. During a cycle of the external driving force $F_d(t)$ the minima of the potential vary. The locations of the minima are depicted in Figure 7.8.

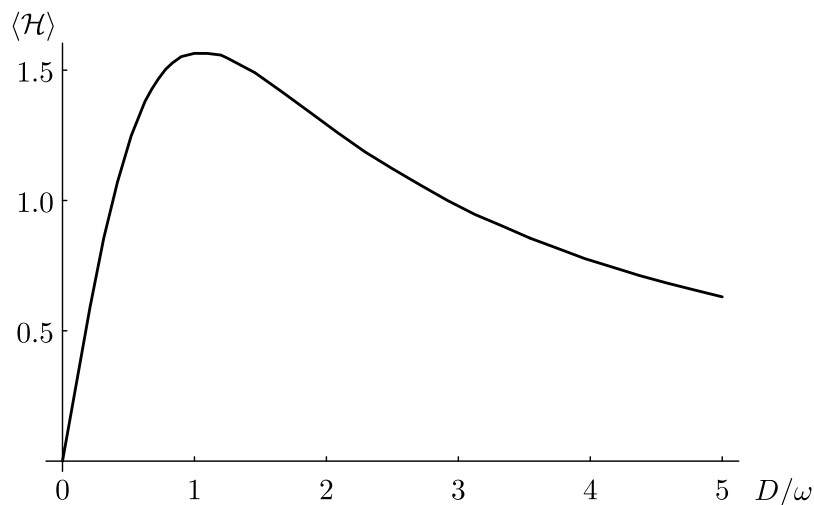


Figure 7.7: D/ω -dependence of the mean hysteresis $\langle \mathcal{H} \rangle$. The calculations were performed with 10000 trajectories simulated according to (7.24). The mean hysteresis $\langle \mathcal{H} \rangle$ was determined after 3 cycles, with $a = 6/\beta$, $k = 6/\beta$ and $2\pi D/\omega = 0.0, 0.1, \dots, 5.0$ with respect to some arbitrary spatial unit. The limit for $\Delta\phi \rightarrow 0$ was performed as outlined in Figure 7.6

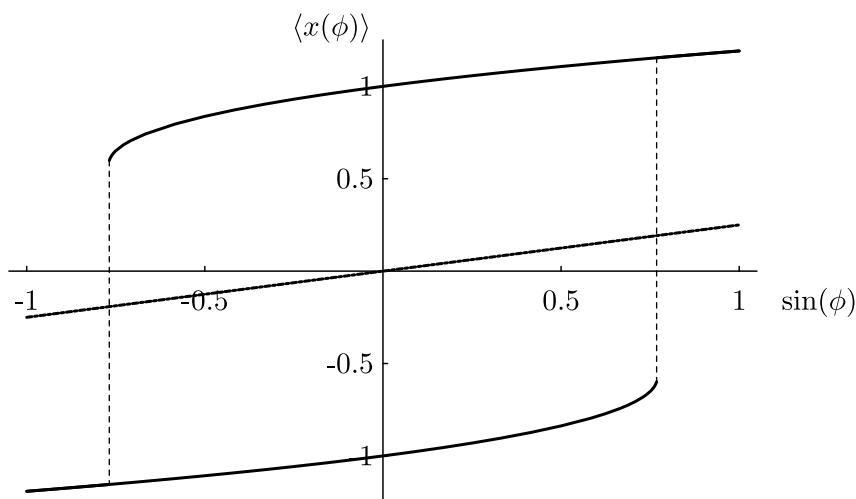


Figure 7.8: The two minima of the potential (7.27) for $k_1 = 1/\beta$, $k_2 = 1/\beta$ and $a = 1/2\beta$ are indicated by the solid lines. If one takes the harmonic approximations of both minima and neglects any transfer rate between them, one obtains the dashed curve through the origin of the coordinate system describing the average of the two potential minima.

The trace of the potential minima, as shown in Figure 7.8, indicate the special features of this hysteresis model. For example, for a phase $\phi = \pi/2$ of the external driving force $F_d(t)$ and for a very low temperature $1/\beta$, i.e., negligible thermal diffusion, a particle in the potential $V(x)$ would be located only in the minimum on the right side. This location corresponds to the right corner of the top solid line in Figure 7.8. Increasing the phase ϕ adiabatically the particle would follow the local minimum. The particle, hence, follows the top solid line from right to left. For ϕ defined through $\sin \phi = -4/\sqrt{27}$ the right minimum disappears. The particle would consequently fall into the minimum on the left depicted by the bottom solid line in Figure 7.8. The particle would follow then the left minimum until this minimum disappears for a ϕ defined through $\sin \phi = 4/\sqrt{27}$ returning to the initial position in the right minimum.

In a simulation with a thermal energy $1/\beta$ comparable to the characteristics of the potential $V(x)$ and with a frequency ω of the driving force $F_d(t)$ comparable to the rate of diffusional crossing of the barrier between minima, the above behaviour gets significantly modified. Due to diffusion we will observe a transition from one local minimum to the other previous to the moment that ϕ assumes the value specified through $\sin \phi = \pm 4/\sqrt{27}$.

In the case of high frequencies ω the transition from left to right and back might not occur all together. For high frequencies particles would not have the time to propagate from one minimum to the other and the hysteresis model would seem to consist of simply two disjunct harmonic potentials at $x = \pm 1$. In this case the adiabatic approximation of a particle ensemble is given by the dashed trajectory in Figure 7.8.

We will now verify these predictions numerically. The equation analog to (7.24), needed for the calculation of Brownian Dynamic trajectories, is

$$x(\phi + \Delta\phi) = x(\phi) - \frac{D\beta}{\omega} (a \sin(\phi) + k_1 x^3 - k_2 x) \Delta\phi + \sqrt{\frac{2D}{\omega}} \Delta\phi. \quad (7.28)$$

A simulation of 10000 trajectories in the potential given by (7.27) with different driving frequencies ω and for a temperature of $\beta = 0.1$ is displayed in Figure 7.12.

In the first case, $D/\omega = 1$, the frequency ω is so high that a substantial transition of the ensemble from the left to the right minimum and vice versa does not occur. This can be discerned in Figure 7.10 which displays the distribution of the ensemble for different phases ϕ in the first column. Consequently the first case resembles the hysteresis of a harmonic potential.

In the second case, $D/\omega = 10$, the frequency ω is low enough for an almost complete shift of the ensemble from the right to the left side and back. The hysteresis, therefore, resembles the adiabatic hysteresis in Figure 7.8. A complete cycle of this case is shown in Figure 7.11.

In the third case, $D/\omega = 100$, the frequency ω is so low that the system has sufficient time for a diffusive transition across the barrier from one local minimum to the other, thus, reducing the hysteresis substantially.

With the trajectories $\langle x(t) \rangle$ as displayed in Figure 7.12 and equation (7.14) one can finally determine the mean hysteresis $\langle \mathcal{H} \rangle$. In contrast to the hysteresis in a harmonic potential, the bistable potential exhibits a strong temperature dependence. To illustrate this one can determine the hysteresis \mathcal{H} for different frequencies ω and temperatures $1/\beta$. The results are displayed in Figure 7.12. One notes that higher temperatures reduce the hysteresis $\langle \mathcal{H} \rangle$. At high temperatures the hysteresis enforcing barrier inbetween the two local minima becomes less significant since the crossing rate over the barrier increases relative to the driving frequency of the external force.

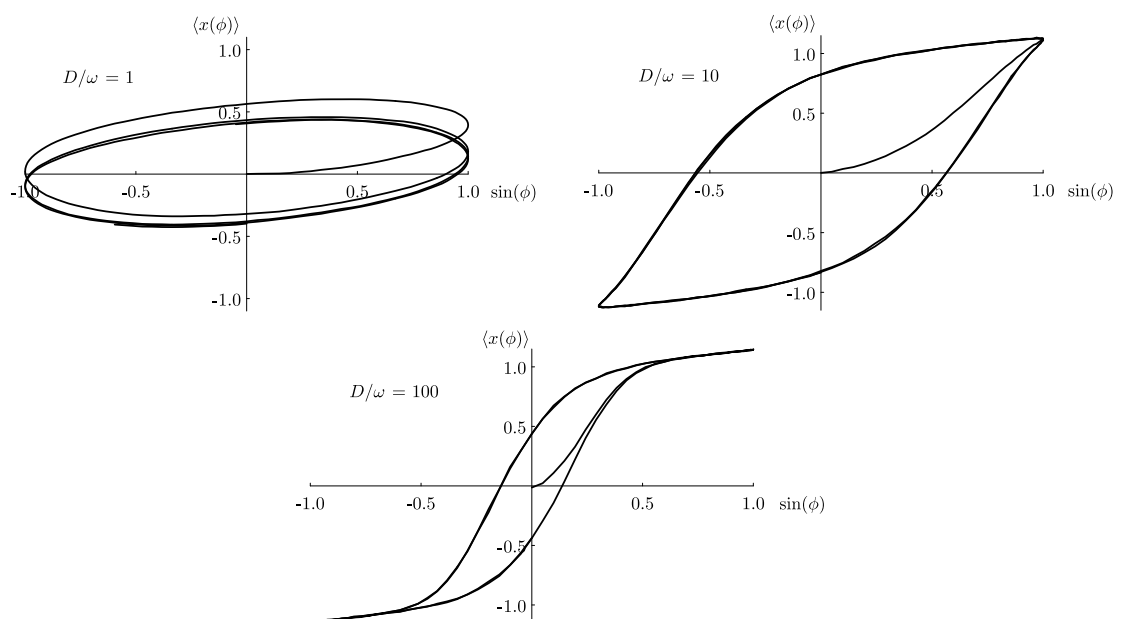


Figure 7.9: Mean trajectory of 10000 particles simulated according to (7.28) with $\Delta\phi = 0.002\pi$, $a = 1/2\beta$, $k_1 = 1/\beta$, $k_2 = 1/\beta$ and $D/\omega = 1, 10, 100$ (arbitrary spatial unit).

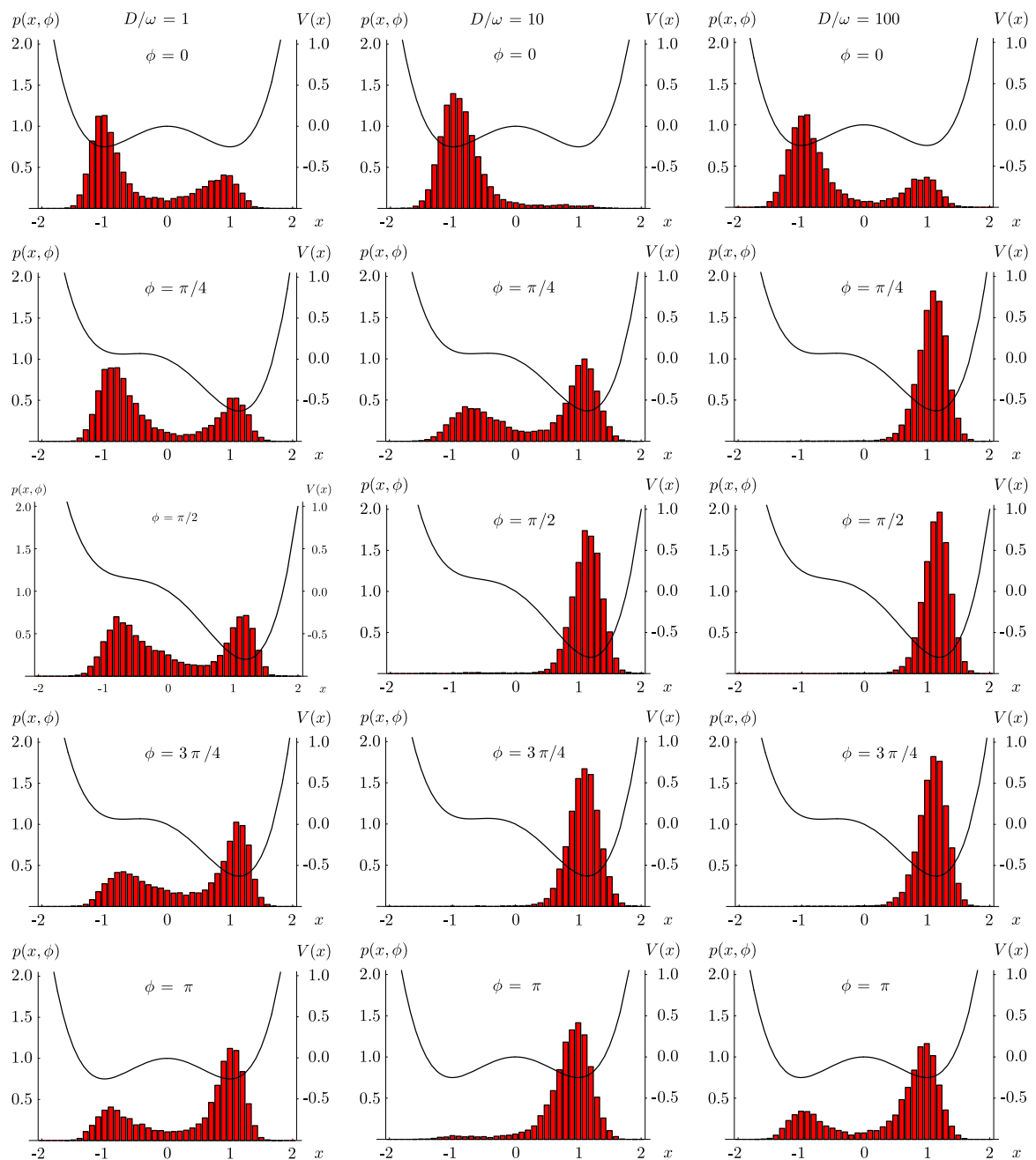


Figure 7.10: These plots display bin counts that approximate the probability distributions of an ensemble in a double potential (7.27) for different driving frequencies ω . The first column depicts the distribution for $\frac{D}{\omega} = 1$ at $\phi = 0, \pi/4, \pi/2, 3\pi/4$, and π . The second column displays the same dynamics for $\frac{D}{\omega} = 10$ and the third column represents the time evolution for $\frac{D}{\omega} = 100$.

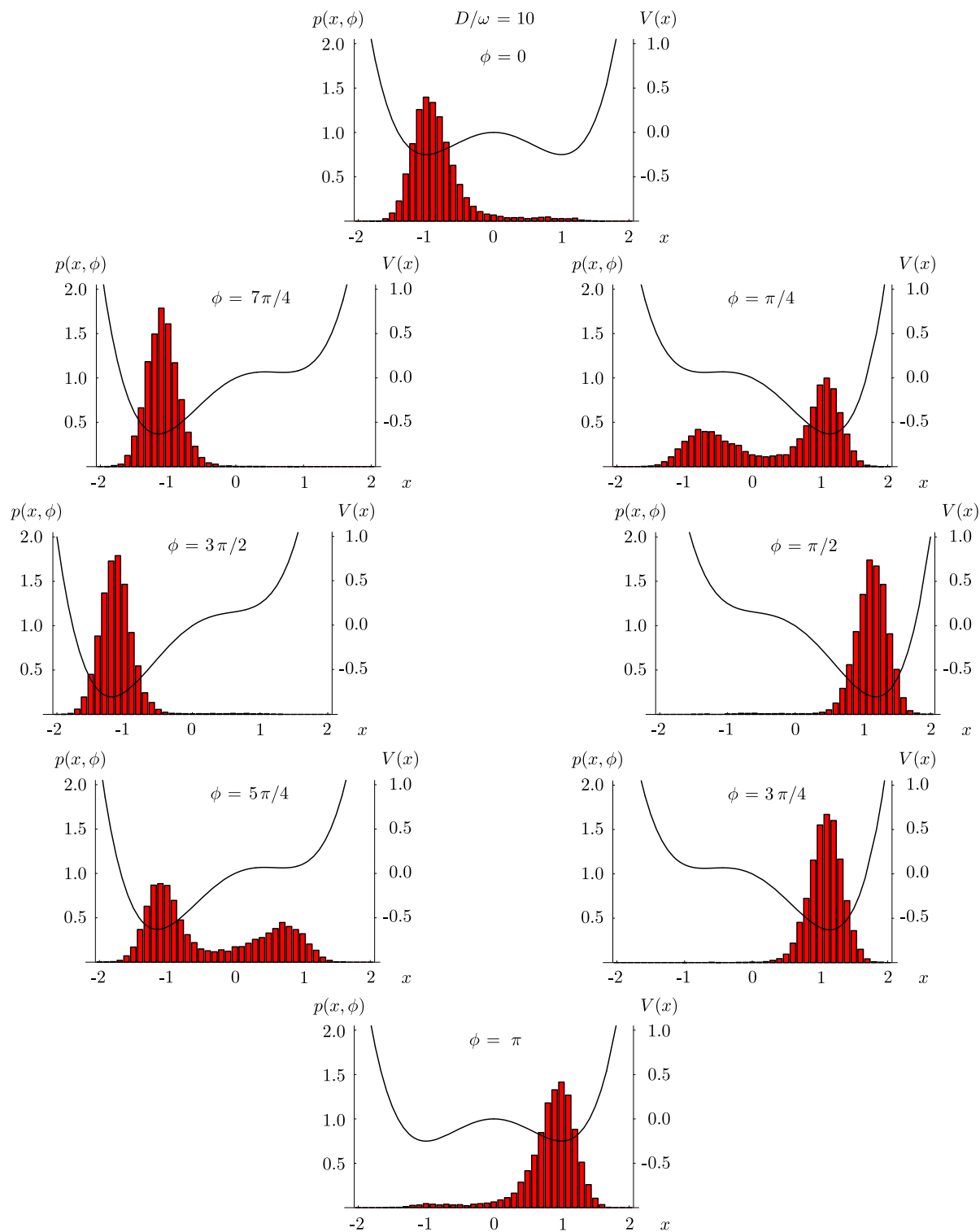


Figure 7.11: These plots display bin counts that approximate the probability distributions of an ensemble in a double potential (7.27) for $D/\omega = 1$. The circle of plots follows the cycle for ϕ from 0 to 2π .

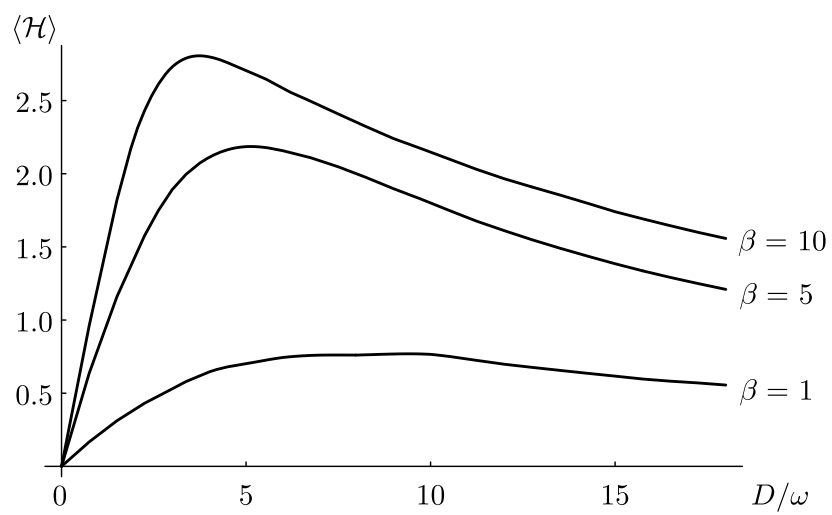


Figure 7.12: D/ω -dependence of the mean hysteresis $\langle \mathcal{H} \rangle$ at different temperatures $1/\beta = 0.1, 0.2,$ and 1 .